# Glutathione Dimerization-Based Plasmonic Nanoswitch for Biodetection of Reactive Oxygen and Nitrogen Species

**Sumit Kumar, Won-Kyu Rhim, Dong-Kwon Lim, and Jwa-Min Nam***

Department of Chemistry, Seoul National University, Seoul 151-747, Korea

**ABSTRACT** Reactive oxygen and nitrogen species (ROS and RNS) are continuously produced in the cellular systems and are controlled by several antioxidant mechanisms. Here, we developed a straightforward, sensitive, and quantitative assay for the colorimetric and spectroscopic detection of various ROS and RNS such as $H_2O_2$, ·OH, $^-$OCl, NO·, and $O_2^-$ using glutathione-modified gold nanoparticles (GSH-AuNPs). A basic principle here is that the GSHs on the AuNP surface can be readily detached *via* the formation of glutathione disulfides upon the addition of ROS and RNS, and destabilized particles can aggregate to generate the plasmonic couplings between plasmonic AuNPs that trigger the red shift in UV—vis spectrum and solution color change. For nonradical species such as $H_2O_2$, this process can be more efficiently achieved by converting them into radical species *via* the Fenton reaction. Using this strategy, we were able to rapidly and quantitatively distinguish among cancerous and normal cells based on ROS and RNS production.

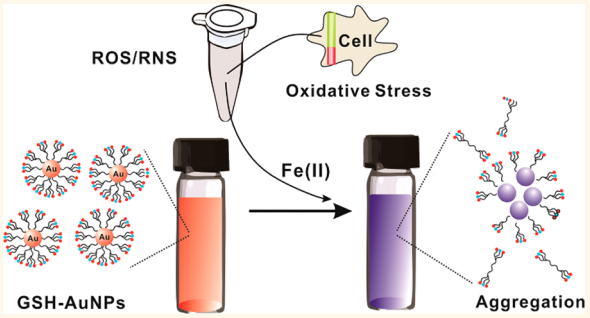


**KEYWORDS:** reactive oxygen species · reactive nitrogen species · plasmonic nanoparticle · glutathione · Fenton reaction

Reactive oxygen and nitrogen species (ROS/RNS) operate as signaling molecules under various physiological conditions and also provide host defense against bacterial and fungal pathogens.[1] These reactive species are normally generated at a low level by human spermatozoa in order to perform its physiological function, but the overproduction of ROS/RNS is involved in the pathogenesis of many diseases such as cardiovascular diseases, cancer, and neurodegenerative diseases.[2,3] Further, the quantitative analysis of ROS/RNS has been used in evaluating the biological toxicity of nanomaterials.[4] Several methods for the detection of ROS/RNS have been developed using fluorophores, chromophores, luminophores,[5] polymer-DNA composites,[6,7] and quantum dots.[8−11] However, these methods have several limitations including tedious operation, complicated setup, limited dynamic range, low sensitivity, use of expensive reagents, and the presence of serious matrix effects, and more rapid, quantitative, reliable, sensitive, and cost-effective detection methods for ROS/RNS have great demand in materials science, biology, and medicine. The plasmonic properties, biocompatibility, and availability of various surface modification chemistries through conjugation with different molecules make gold nanoparticles (AuNPs) excellent optical biosensing substrates.[12−26] Recently, a few papers have been published about the ROS detection using AuNPs, but the detection target was mainly limited to a specific type of ROS such as $H_2O_2$ in those reports.[27−31,11]

Here, we report a method that utilizes glutathione(GSH)-modified plasmonic nanoparticles and their plasmonic couplings, induced by the ROS/RNS-activated dimerization of GSHs to GSH disulfides (GSSGs) and the Fenton reaction, to detect the subtle changes in the concentration of various ROS/RNS in one solution (Scheme 1). It was shown this straightforward GSH-AuNP-based method can detect $H_2O_2$, ·OH, $^-$OCl, NO·, and $O_2^-$. We further applied this method to the quantitative detection of oxidative stress from normal and cancerous cells. A major working principle for this method is that the ROS/RNS-based dimerization of GSH to GSSG on the AuNP surface induces the detachment of GSSGs

* Address correspondence to jmnam@snu.ac.kr.

Received for review November 12, 2012 and accepted February 28, 2013.

**Published online February 28, 2013**
**10.1021/nn305250p**

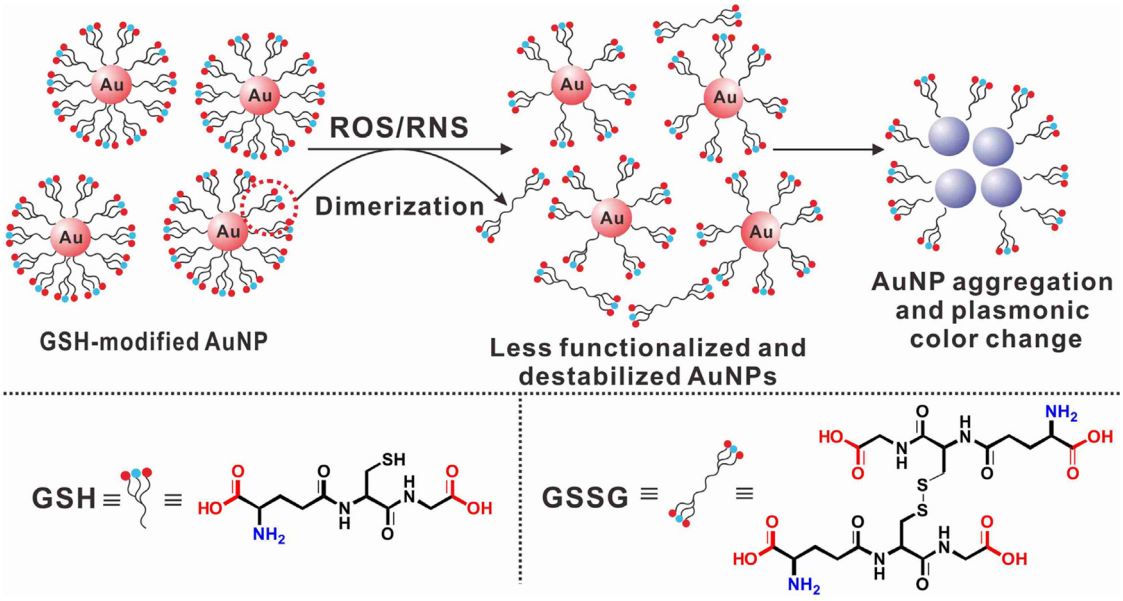


**Scheme 1. The reaction between the glutathione-modified Au nanoparticles and ROS/RNS and the plasmonic coupling-based colorimetric ROS/RNS detection.**

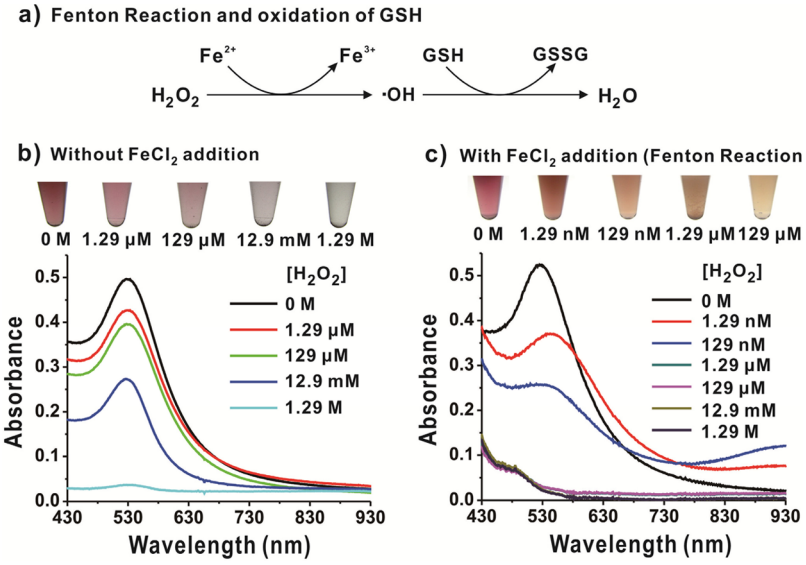


**Figure 1. The Fenton reaction-aided $H_2O_2$-detection using the GSH-AuNP probes. (a) $FeCl_2$-catalyzed oxidation of GSH (Fenton reaction). (b) UV−vis absorption spectra and corresponding solution color images of the GSH-AuNP solutions after the addition of a series of different concentrations of $H_2O_2$. (c) UV−vis absorption spectra and corresponding solution color images of the GSH-AuNP solutions after the addition of a series of different concentrations of $H_2O_2$ and 10 mM $FeCl_2$ solution.**

and subsequent AuNP aggregation and plasmonic couplings between particles (Scheme 1). GSH has thiol, carboxyl, and amine groups and is water-soluble and biocompatible.[32−36] In our approach, the thiol group in GSH structure was used to stably conjugate GSHs to AuNPs to form the GSH-AuNPs. When the GSH-AuNPs are exposed to the ROS/RNS in radical forms, the GSH molecules, present on AuNPs, readily react with ROS/RNS to form GSSGs which are unable to coordinate to AuNPs because of steric hindrance caused by bulky groups around sulfur atoms of GSSGs.[37] The ROS/RNS-driven formation of GSSGs induces the detachment of these ligands from AuNPs, resulting in the destabilization of the GSH-AuNPs. This eventually induces AuNP aggregation and plasmonic couplings between plasmonic AuNPs[10] for solution color change and red shift in the UV−vis spectrum (Scheme 1). In the case of non-radical species ($H_2O_2$ in this case), it is necessary to convert them into radical species for making them more reactive with GSHs in forming GSSGs. For this purpose, we used the Fenton reaction—$FeCl_2$-catalyzed decomposition of $H_2O_2$.[1,38,39] As shown in Figure 1, the Fenton reaction can readily convert $H_2O_2$ into ·OH, and a perfectly biocompatible water molecule is produced when the reaction is completed (Figure 1a). In cell experiments, we found that these GSH-AuNP probes can be

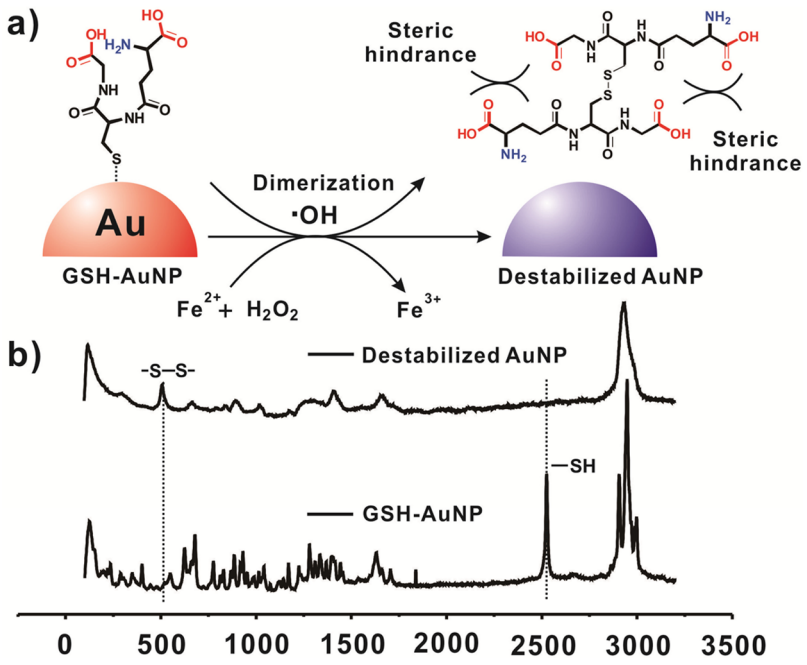


**Figure 2. Raman spectroscopic study for the destabilization of GSH-AuNPs by the Fenton reaction. (a) Schematic diagram shows the dimerization of glutathione on gold nanoparticle surface after reacting with hydroxyl radicals. (b) The Raman spectra of GSH-AuNPs and destabilized gold nanoparticles.**

readily internalized by cells and were distributed outside cell nucleus. Finally, we used these probes for detecting total ROS/RNS levels from cell lysates and compared the results from six different cell lines (three normal and three cancerous cell lines).

## RESULTS AND DISCUSSION

**Synthesis of GSH-AuNPs.** In a typical experiment, the GSH-AuNPs were prepared by a literature method in 10 mM phosphate buffer (PB, pH 7.4).[33] Synthesized probes were characterized by the UV−vis spectroscopy (Agilent UV−visible spectrophotometer G1103A), transmission electron microscopy (JEOL JEM-1400 transmission electron microscope), and dynamic light scattering and zeta potential measurements (Zetasizer Nano, Malvern Instruments Ltd., England) (please see the Experimental Section and Supporting Information for details). The stability of our probes was tested under various pH conditions, and we confirmed that they are stable from pH 5.0 to pH 8.0 (Figure S2 in the Supporting Information).

**Detection of $H_2O_2$ by Using GSH-AuNPs with or without the Fenton Reaction.** First, in testing the Fenton reaction for GSH-AuNPs, a series of different concentrations of $H_2O_2$ were added to 47 nM GSH-AuNPs in 100 $\mu$L of PB (10 mM, pH = 7.4). After incubating these mixtures at 25 °C for 2 h, solution color was monitored and UV−vis spectra were recorded (Figure 1). When no $FeCl_2$ was added, the absorption intensity of the GSH-AuNPs at 525 nm gradually decreases with gradual increase in $H_2O_2$ concentration and solution color was changed from purple to blue (Figure 1b). The $H_2O_2$ detection range was from 1.29 $\mu$M to 1.29 M. Importantly, when 10 mM $FeCl_2$ (10 $\mu$L) was added to the probe solution, assay sensitivity was dramatically increased and as low as 1.29 nM $H_2O_2$ was detected (Figure 1c). Interestingly, solution color was changed from purple to yellowish-brown due to AuNP aggregation and increase in $Fe^{3+}$ ions as $H_2O_2$ concentration increases. In a control experiment, we found that the sole addition of $Fe^{2+}$ to the GSH-AuNPs in the absence of ROS/RNS did not lead to aggregation of the GSH-AuNPs or any noticeable changes in the color or spectra of the resulting AuNPs (Figure S3 in the Supporting Information).

To probe our proposed mechanism for ROS/RNS detection, we used the Raman spectroscopy in characterizing the glutathione molecules on the Au surface. The Raman spectroscopy is a technique that can characterize the vibrational modes of individual bonds and offer insight in chemical structure, and Raman signals can be easily detected in our case because of the surface-enhanced Raman scattering for the molecules on the plasmonic gold surface. In Figure 2a, hydroxyl radicals, generated from the Fenton reaction, react with GSH molecules present on the gold surface and form GSSGs, which are unable to coordinate to AuNPs because of the structural change and steric hindrance, caused by bulky groups around sulfur atoms of GSSGs. The Raman experiments (inVia Raman Microscope, Renishaw, Wotton-under-Edge, UK) were performed to follow the Fenton reaction-based GSSG formation (25 °C, Ar laser of 514.5 nm laser line with power 50 mW). In Figure 2b, the Raman spectra for GSH-AuNPs and final product, respectively, are shown. We observed the

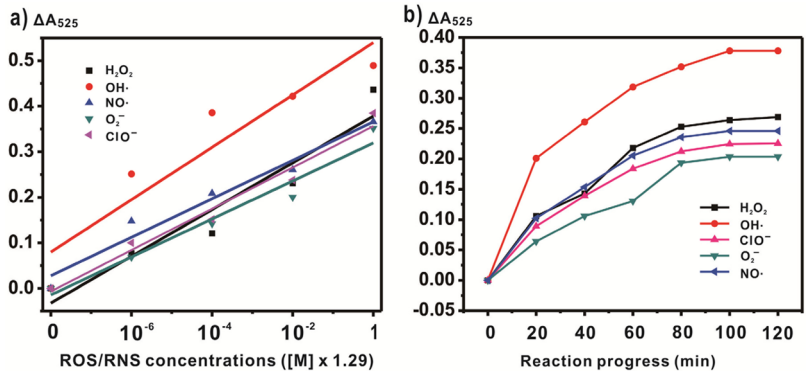


**Figure 3. (a) Plots of reaction kinetics for change in $\Delta A_{525}$ as a function of (a) ROS/RNS concentration upon the treatment with the GSH-AuNPs for 2 h or (b) reaction progress (min) for various ROS/RNS at a constant concentration (1.29 mM) upon the reaction with the GSH-AuNPs.**

bands at 2579 $cm^{-1}$ (S—H stretching), 678 $cm^{-1}$ (C—S stretching), 1706 $cm^{-1}$ (C═O stretching), 1632 $cm^{-1}$ (amide stretching), and 2890 $cm^{-1}$ (O—H stretching), respectively, for GSH-AuNPs. For the product, we observed the bands at 511 $cm^{-1}$ (S—S stretching), 679 $cm^{-1}$ (C—S stretching), 1708 $cm^{-1}$ (C═O stretching), 1640 $cm^{-1}$ (amide stretching), and a broad band at 2881 $cm^{-1}$ (O—H stretching). For the product case, we did not observe the thiol (S—H) peak, which indicates the GSH molecules on the gold surface were oxidized to GSSGs. Further, we performed an X-ray photoelectron spectroscopy (XPS) experiment (ThermoVG, UK) to characterize the number of ligands on each AuNP surface. By comparing the atomic ratios of sulfur to gold before and after the reaction between GSH-AuNPs and hydroxyl radicals, generated from the Fenton reaction, we observed the change in the number of ligands per particle. From the XPS results it was found that the atomic ratio (sulfur/gold) during the reaction decreased from 5.89 to 0.47. To test the long-term stability of the ligands on probes, we prolonged the reaction time up to 24 h. There is only negligible increase in the atomic ratio (sulfur/gold) to 0.51. All these results point out that the sulfur atoms in bulky GSSGs in solution did not coordinate back to AuNPs once they were released from particles. The formation of GSSG was further verified by the mass spectrometry (Finnigan MSQ Plus Surveyer MS system with photodiode array detector using electron spray ionization), where a molecular ion peak corresponding to GSSG appeared at $m/z$ = 612.81 (Figure S4 in the Supporting Information). Finally, the $^1$H NMR (500 MHz) (Varian Inova-500, Varian Assoc., Palo Alto, USA) analysis of GSH-AuNPs before and after ROS/RNS addition confirmed the quantitative conversion of GSH to GSSG in the presence of ROS/RNS (Supporting Information, Figure S5).

**Detection and Quantification of Various ROS/RNS Using GSH-AuNP Probes.** Next, we used the GSH-AuNP probes for detection of many different kinds of biologically relevant ROS/RNS species including hypochlorite ($ClO^-$), nitric oxide (NO·), superoxide ($O_2^-$), $H_2O_2$, and ·OH. In our experiments, NO· was generated from $NaNO_3$ and diethylammonium(*Z*)-1-(*N*,*N*-diethylamino)diazen-1-ium-1,2-diolate, and $O_2^-$ was generated from xanthine oxidase and xanthine. NaOCl was used as the source of $ClO^-$ (see the Experimental Section for more details). In each case, 10 $\mu$L of ROS/RNS was added to 90 $\mu$L of 47 nM GSH-AuNP solution, and the resulting solution was incubated on an orbital shaker at 25 °C for 2 h. It should be noted that ·OH was generated from $H_2O_2$ by the addition of $FeCl_2$ (Figure 1). The GSH-AuNPs showed good response to all these ROS/RNS with high detection sensitivity. Figure 3a shows the dependence of $\Delta A_{525}$ as a function of ROS/RNS concentration where $\Delta A_{525}$ is the difference between optical densities in the absence and presence of ROS/RNS at 525 nm, respectively. These results show a linear relationship between $\Delta A_{525}$ and ROS/RNS concentration with a wide dynamic range ($R^2$ = 0.9288, 0.8439, 0.90687, 0.98729, and 0.95144 for $H_2O_2$, ·OH, $O_2^-$, NO·, and $ClO^-$, respectively). The minimum detectable concentrations for $O_2^-$, NO·, and $ClO^-$ were found to be 1.29 mM, 129 $\mu$M, and 1.29 $\mu$M, respectively. The detection sensitivity of ROS using our method was comparable to a luminal-based assay.[40] It should be noted that, although $O_2^-$ is a primary source of ROS/RNS in biological systems, this species is least reactive for our probe. Figure 3b shows the reaction kinetics results for each ROS/RNS, where corresponding $\Delta A_{525}$ values were plotted as a function of reaction time. For this study, the identical concentration for all the species (1.29 mM in 10 mM PB at pH = 7.4) was used, and the reaction progresses for each species were monitored up to 120 min at 25 °C. The results revealed that all the reactions were nearly completed at ~80 min. All the reactions did not progress any further after 100 min. More reactive ROS/RNS molecules ($H_2O_2$, ·OH, and $ClO^-$), which are relatively stronger oxidants than NO· and $O_2^-$, showed faster kinetics and more changes in $\Delta A_{525}$ than NO· and $O_2^-$,[1,38] and these results validate the quantification capability of our assay.

**Effect of Temperature on Reaction Kinetics of GSH-AuNPs with Hydrogen Peroxide.** Other than room temperature, the other relevant temperature is physiological temperature,

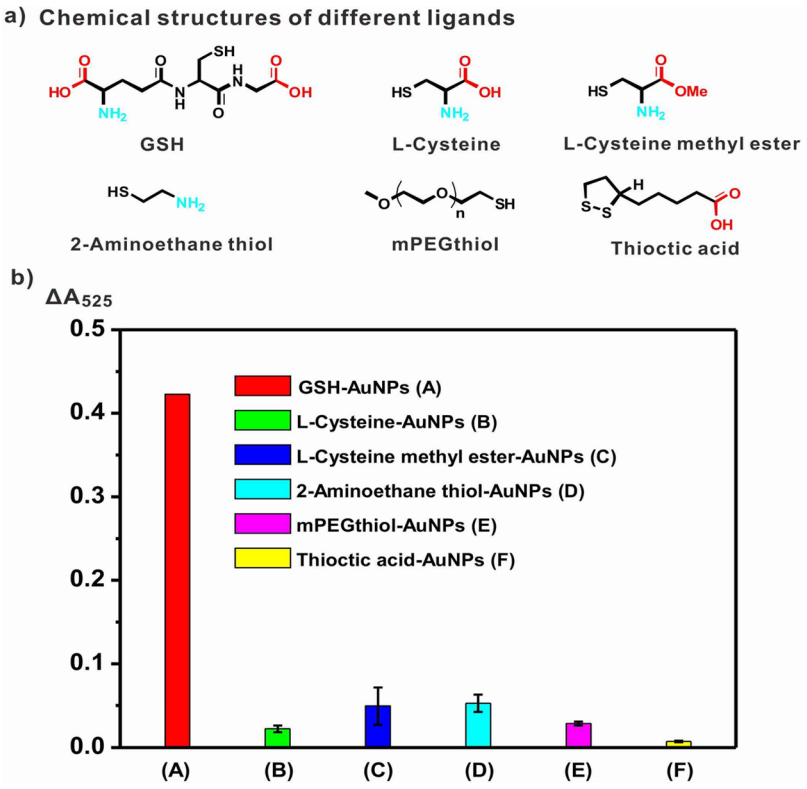


**Figure 4. Comparison of GSH-AuNPs with other thiolated ligands for $H_2O_2$ detection: (a) The chemical structures of non-GSH thiolated ligands; (b) $\Delta A_{525}$ values for differently functionalized AuNPs upon the treatment with 12.9 mM $H_2O_2$.**

37 °C. Actually, we used our probes at 37 °C for cell assays. We compared probes with respect to solution color, surface charge (zeta potential), and particle size at room temperature and 37 °C, respectively. There was only a little change in the zeta potential and particle size with no solution color change and no particle aggregation when temperature was changed from 25 to 37 °C (see Figure S6 in the Supporting Information). Further, the cell assays with GSH-AuNPs were performed at 37 °C, and the results are shown in the latter part of this paper.

**Comparison of GSH with Other Thiolated Ligands.** Next, we examined the specificity in the reaction between ROS/RNS and GSH on AuNP surface by interacting other thiolated group-modified AuNPs with ROS/RNS (Figure 4a). For this study, we selected a variety of thiolated ligands including cysteine, methyl cysteine, 2-aminoethanethiol, mPEG-SH (MW 5000), and thioctic acid. These functional ligands were modified to AuNPs based on reported procedures (see the Experimental Section for details)[41−43] and characterized by the UV−visible spectroscopy, TEM, dynamic light scattering and zeta potential measurements. It should be noted that commercially available 15-nm AuNPs were used for the synthesis of mPEG-SH-capped AuNPs. For each case, 90 $\mu$L of 47 nM AuNP probe solution was mixed with 10 $\mu$L of 12.9 mM $H_2O_2$, and the reaction mixture was stirred at 25 °C for 2 h. After 2 h reaction, the UV−vis absorbances at 525 nm before and after the addition of ROS/RNS were recorded and compared. Importantly, as shown in Figure 4b, the addition of $H_2O_2$ had little effect on change in the absorbance at 525 nm for all non-GSH-modified AuNPs, unlike the case for GSH-AuNPs. This shows that our assay strategy does not work for AuNP probes with other thiolated ligands but works only for GSH-modified AuNPs that can form dimeric GSSG upon the addition of ROS/RNS species. This result could be attributed to its structural feature and low reduction potential (50 mV or lower) of GSH when compared to other thioled ligands such as cysteine.[44,45]

**TABLE 1. Cell Lines Used in This Study**

| | | | |
|---|---|---|---|
| mouse | myoblast cell | $C_2C_{12}$ | normal |
| | fibroblast cell | 3T3-L1 | normal |
| | fibroblast cell | NIH-3T3 | normal |
| human | hepatoma cell | Hep3B | cancerous |
| | lung cell | A549 | cancerous |
| | cervical cell | HeLa | cancerous |

**GSH-AuNPs as Cell Assay Probes.** Our next goal was to exploit potential for the use of our GSH-AuNPs in monitoring and quantifying the ROS/RNS amount from normal and cancerous cells. Several reports suggest that many types of cancerous cells generate the increased amount of ROS/RNS due to oncogenic stimulation, increased metabolic activity and mitochondrial malfunction.[46−50] Therefore, this oxidative stress of cancer cells can be used as a hallmark for the diagnosis by differentiating normal cells from cancerous cells.[51,52]

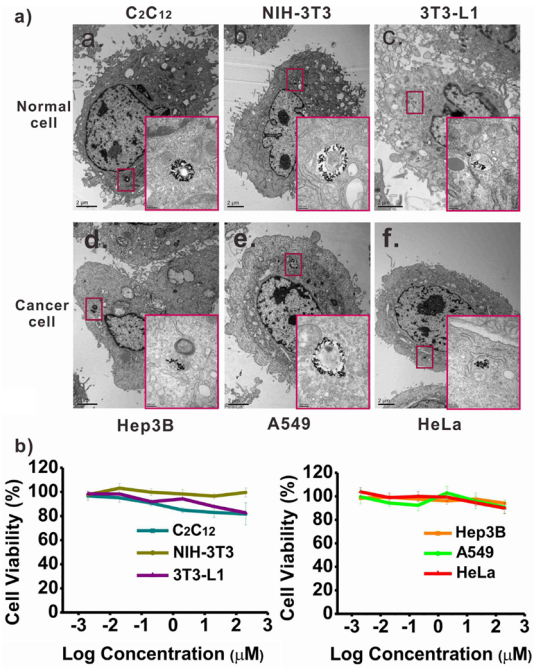


**Figure 5. GSH-AuNPs with cells. (a) The GSH-AuNP probes are internalized into both normal and cancerous cells. Up taken probes were characterized by the TEM after cell fixation. (b) The cell viability results obtained using the Cell Counting Kit after 2-day incubation with varying concentrations of GSH-AuNP probes. The error bars represent the standard deviations based on three independent measurements.**

It should also be noted that obtaining the quantitative information about a change in ROS/RNS level among normal cells or cancerous cells could be valuable for studying oxidative stress in biochemistry and cell biology.[53] As a control experiment, we first tested the response of our GSH-AuNPs probes for the mixture of different kinds of ROS/RNS in one solution [10 $\mu$L of a solution with 12.9 $\mu$M $H_2O_2$, $\cdot OH$, $O_2^-$, NO$\cdot$, and $ClO^-$ was added to 90 $\mu$L of 47 nM GSH-AuNPs in 10 mM PB solution at pH = 7.4]. After this mixture was incubated at 25 °C for 2 h, UV−vis spectrum was recorded. The result showed significant decrease in the absorption intensity at ~525 nm (Figure S7 in the Supporting Information).

Next, we conducted the cellular uptake experiments of the GSH-AuNPs with six different cell lines (listed in Table 1, normal cells: 3T3-L1, NIH3T3, and C2C12; cancerous cells: A549, HeLa, and Hep3B). The cellular uptake of the GSH-AuNPs was characterized by the cell fixation and subsequent TEM imaging after the incubation of the GSH-AuNPs with cells (see the Experimental Section for more details). As shown in Figure 5a, many GSH-AuNPs were found inside the cell for all of six cell lines, but it should be noted that the GSH-AuNPs were not found inside the cell nucleus. These results confirm that the GSH-AuNPs can be readily internalized by both cancerous and normal cells and these probes have potential as ROS/RNS detection probes inside the cell.

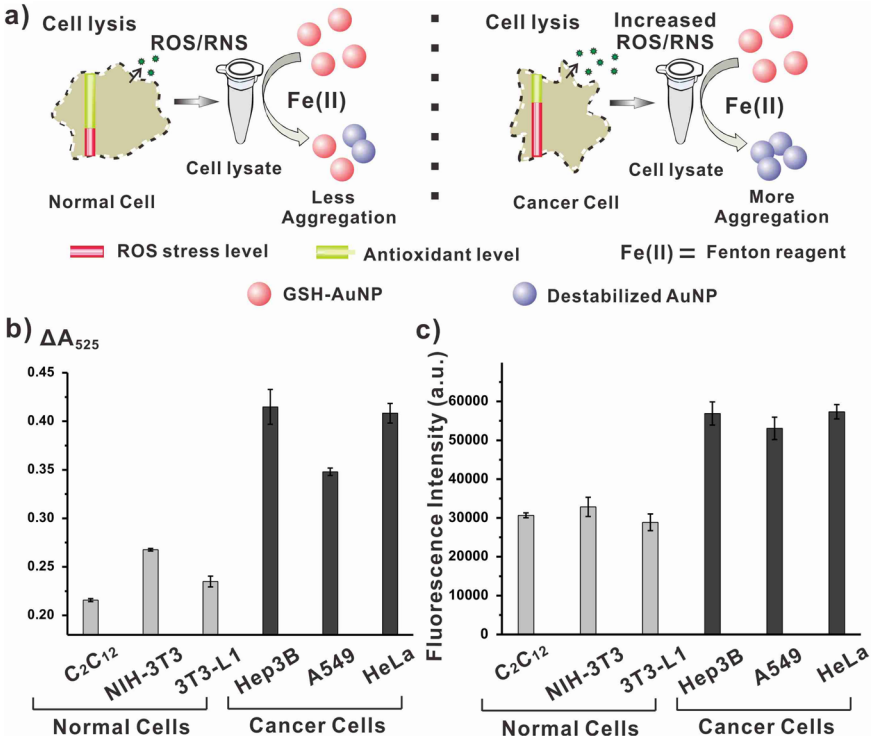


**Figure 6. (a) Changes in redox balance for normal and cancerous cells and subsequent detection of ROS/RNS from cells using the GSH-AuNP probes. (b) Quantitative comparison of ROS/RNS assay results from various normal and cancerous cells using GSH-AuNPs probes. (c) ROS/RNS assay results from various normal and cancerous cells using a commercially available *in vitro* ROS/RNS kit. The error bars represent the standard deviations based on three independent measurements.**

Interestingly, although the probes have highly negative charges on the surface (zeta potential = −39.76 mV), there is no significant hindrance for the GSH-AuNPs in entering through cellular membrane. This could be due to the ionic screening effect by various serum proteins in cell growth medium, and other cell membrane components could play important roles for the endocytosis of the probes.[54] Next, we performed the cytotoxicity tests for the GSH-AuNPs with six different cell lines using the Cell Count Counting Kit assay.[55] A wide range of GSH-AuNP concentrations (2 nM to 200 $\mu$M) showed no or little cytotoxicity for all the tested cell lines (Figure 5b; see the Experimental Section for experimental details). These GSH-AuNPs were found to have little or no toxicity to live cells even at high concentrations.

**Detection of ROS/RNS in Normal and Cancerous Cells.** In a typical experiment, six cell lines (Table 1: normal cells, 3T3-L1, NIH3T3, and C2C12; cancerous cells, A549, HeLa and Hep3B) were cultured in serum-confluent medium for 3 days, respectively, and the same number of cells ($5 \times 10^5$ cells in 10 $\mu$L of PB of 10 mM at pH 7.4) for each case were detached from the cell incubating plate (6-well clear multiple well plates, Corning, Tewksbury, MA, USA), followed by cell lysis using the M-PER mammalian protein extraction reagent (Pierce, Rockford, IL, USA). Cell debris were removed from cell lysate using centrifugation, and the remaining solution was co-incubated with 90 $\mu$L of 47 nM GSH-AuNPs in 10 mM PB solution in the presence of 10 mM $FeCl_2$ at 37 °C for 4 h. The supernatant from cell-lysate solution that was coincubated with GSH-AuNPs was used for the UV−vis measurement (see the Experimental Section for experimental details). The spectral change in the absorbance at 525 nm was measured with the UV−vis spectrophotometer. We were able to observe the change in absorbance depending on cell type. Overall, as shown in Figure 6b, larger $\Delta A_{525}$ values were observed for all the cancerous cells than the values for the normal cells (Figure 6), and this result agrees well with other literatures.[20] The error bars are relatively small, and detection of ROS/RNS was successfully performed using only one type of probe. To further validate our results, a commercially available *in vitro* ROS/RNS assay (OxiSelect, Cell biolabs, INC., San Diego, CA, USA) was also conducted, and the results were compared to the GSH-AuNP assay results. The OxiSelect assay is a fluorescent signal-based method for measuring total ROS/RNS free radical activity.[56] Importantly, the ROS/RNS detection results from the commercial assay showed a very similar tendency as observed in our GSH-AuNP assay results (Figure 6b,c; see the Experimental Section for details).

## CONCLUSION

In summary, we developed a simple and straightforward strategy to detect a wide range of different ROS/RNS molecules including NO·, $^{-}$OCl, $O_2^{-}$, $H_2O_2$, and ·OH *via* the dimerization of GSH on AuNPs surface to GSSG upon the addition of ROS/RNS. This ROS/RNS-mediated dimerization of GSH induces the detachment of GSH from AuNPs and destabilizes AuNPs to provoke particle aggregation that results in plasmonic couplings between AuNPs. These plasmonic couplings were readily detected with the naked eyes or UV−vis spectrophotometer. This chemistry works efficiently with radical forms of ROS/RNS, and the Fenton reaction boosted the detection sensitivity for nonradical species such as $H_2O_2$ by converting it to ·OH. Moreover, it was shown that other non-GSH thiol molecule-modified AuNP probes were not sensitive to the presence of ROS/RNS, indicative of high specificity of this method to GSH-AuNPs. Finally, we showed that GSH-AuNPs probes can be used to quantify the amount of ROS/RNS from normal and cancerous cells to measure oxidative stress in cell. Our results proved that these probes can be internalized by cells and have no or little cytotoxicity even at high probe concentrations (over $\mu$M level). These show that the GSH-AuNPs can be potentially used as ROS/RNS detection probes inside the cell. Our assay quantitatively detected higher amount of ROS/RNS from cancerous cells than from normal cells, which agrees well with oxidative stress-based results reported in other literatures, and these results were matched well by commercially available assay kit-based results. These versatile and simple ROS/RNS detection probes and assay platform offer new opportunities in detecting and quantifying the amount of ROS/RNS and relating ROS/RNS detection with oxidative stress in cells, differentiating normal cells from cancerous cells,and various other studies in ROS/RNS-related cell signaling and phenotypic changes.

## EXPERIMENTAL SECTION

**Chemicals.** Gold nanoparticles (15 nm in diameter) were purchased from Ted pella (Redding, CA, USA) and used without further purification. Tetrachloroauric acid, glutathione, ferrous chloride, 2-aminoethanethiol, *N*,*N*-dimethylformamide, deuterium oxide, L-cystein methyl ester, and L-cystein were purchased from Aldrich (St. Louis, MO, USA). HEPES, toluene, tetra-*n*-octyl ammonium bromide, 6,8-dithioctic acid, xanthine oxidase, and xanthine were purchased from Sigma (St. Louis, MO, USA). Sodium borohydride, hydrogen peroxide, sodium nitrate, and hydrochloride were purchased from Daejung chemical and metals (South Korea). *m*-PEG-SH was purchased from Laysan Bio, Inc. (Tower Drive Arab, AL). NANOpure water (>18.0 MΩ), purified using a Milli-Q water purification system, was used for all the experiments.

**Preparation of GSH-AuNPs.** GSH-AuNPs were synthesized according to literature procedures with slight modification.[33] An aqueous solution of tetrachloroauric acid ($HAuCl_4 \cdot 3H_2O$, 1 mL, 0.025 M) was added to GSH (7.8 mL, 0.019 M) dissolved in 10 mM sodium phosphate buffer (PB, pH 7.4) (adjusted by 1 M NaOH). The solution turned clear after continuous stirring for 30 min. Then, a freshly prepared $NaBH_4$ solution (2 mg/mL dissolved in

ice-cold water, 10-fold molar excess) was rapidly added with vigorous stirring (*ca.* 1200 rpm). The solution immediately became dark, indicating the reduction of gold salt and formation of nanoparticles. The reaction was allowed to proceed for 12 h at 25 °C. Excess ligands were removed from the solution by centrifugation at 10000 rpm for 10 min and repeated washing by buffer solution. The obtained gold nanoparticle precipitate was dispersed in 100 mL of PB (10 mM, pH 7.4) and stored at 4 °C for further characterization.

**Preparation of 2-Aminoethanethiol-AuNPs.** A 400 mL aliquot of 213 mM 2-aminoethanethiol was added to 40 mL of 1.42 mM $HAuCl_4$. After the mixture was stirred for 20 min at 25 °C, 10 mL of 10 mM $NaBH_4$ was added, and the mixture was vigorously stirred for 10 min at 25 °C in the dark. After further mild stirring, the sample was stored in the dark at 5 °C and used within 2 months.[41]

**Preparation of Thioctic Acid-AuNPs.** Au clusters were synthesized in toluene by the two-phase reduction of aqueous $HAuCl_4$ (3 mL, 30 mM, Aldrich), transferred to the organic phase using tetra-*n*-octylammonium bromide (TOABr) in toluene (8 mL, 50 mM, Fluka), and reduced with aqueous sodium borohydride (2.5 mL, 0.4 M, Aldrich). Cluster derivatization was carried out by overnight incubation in a 0.1 M solution of 6,8-dithioctic acid (TA, Sigma) in toluene. The carboxylic acid-terminated clusters were insoluble in toluene and were separated by centrifugation, and washed several times with toluene and once with 1-propanol to remove reaction byproducts. The purified clusters were redissolved in an aqueous solution of pH 10 containing 20 mM of HEPES [*N*-(2 hydroxyethyl)piperazine-*N*′-(2-ethanesulfonic acid), Sigma].[42]

**Preparation of mPEGSH-AuNPs.** An aqueous solution containing $1.36 \times 10^{-7}$ moles of mPEGSH (MW 5000), previously sonicated for 15 min, was added under vigorous stirring to 10 mL of commercially available 15-nm gold sphere. The mixture was allowed to react for overnight. PEG-modified particles were then centrifuged (10000 rpm) twice to remove the excess mPEGSH and redispersed in 4 mL of deionized water.

**Preparation of L-Cysteine-AuNPs.** A $10^{-4}$ M aqueous solution (100 mL) of chloroauric acid ($HAuCl_4$) was reduced by 0.01 g of sodium borohydride ($NaBH_4$) at 25 °C. The gold nanoparticles were stabilized by the addition of an aqueous solution of L-cysteine to the hydrosol to yield a final concentration of $10^{-4}$ M cysteine in solution. The pH of the cysteine-capped gold colloidal solution was 9. At this pH, the cysteine molecules on the surface of the gold nanoparticles would be negatively charged (pI of cysteine, 5.06), thus stabilizing the nanoparticles electrostatically.[43]

**Preparations of L-Cystein Methyl Ester-AuNPs.** A 1.42 mM aqueous solution (50 mL) of chloroauric acid was mixed with 213 mM aqueous solution (400 $\mu$L) of L-cystein methyl ester and the reaction mixture was stirred for 20 min at 25 °C. Then the solution was reduced by the addition of 10 mM aqueous solution (10 $\mu$L) of $NaBH_4$. The reaction mixture was stirred for overnight. After further mild stirring, the sample was stored in the dark at 5 °C and used within 3 months.

**Generation of ROS/RNS.** (a) $H_2O_2$: $H_2O_2$ was diluted appropriately by 10 mM PB at pH 7.4. Then, a $H_2O_2$ stock solution in buffer was prepared. To a solution of 90 $\mu$L of GSH-AuNPs in 10 mM PB at pH 7.4, stock solution was added at 25 °C, and then the solution was analyzed by UV−vis absorption spectra after 2 h. (b) Generation of ·OH: 10 mM solution of $FeCl_2$ was prepared in 10 mM PB at pH 7.4. After 80 $\mu$L of GSH-AuNPs and 10 $\mu$L of $H_2O_2$ were mixed in PB (10 mM, pH 7.4), 10 $\mu$L of $FeCl_2$ solution was added at 25 °C. UV−vis absorption spectra were measured after 2 h. (c) Generation of $^-$OCl: NaOCl solution was diluted appropriately in 0.1 M NaOH aq. To a solution of 90 $\mu$L of GSH-AuNPs in 10 mM PB (pH 7.4), 10 $\mu$L of $^-$OCl solution was added at 25 °C, and UV−vis absorption spectra was measured after 2 h. (d) Generation of $O_2^-$: Xanthine oxidase (XO) was dissolved in PB (10 mM, pH 7.4). Xanthine was dissolved in DMF. To a solution of 90 $\mu$L of GSH-AuNPs in PB (10 mM, pH 7.4), XO solution and xanthine solution (final concn, 33 $\mu$M, containing 6.7% DMF as a cosolvent) were added at 25 °C, and UV−vis absorption spectra were measured after 2 h. (e) Generation of NO·: A solution of $NaNO_3$ in PB (10 mM, pH 7.4) and DEANO (DEA NONOate; diethylammonium (*Z*)-1-(*N*,*N*-diethylamino) diazen-1-ium-1,2-diolate) in 0.01 M NaOH was used. To initiate decomposition of the NONOate, 5 $\mu$L of 1.0 M HCl was added to bring the solution to approximately pH 4. After 1 h, 5 $\mu$L of 1.0 M NaOH was added to bring the solutions up to approximately pH 7.4. The solutions were then added to 90 $\mu$L of GSH-AuNP in PB (10 mM, at pH 7.4).

**Cell Cross-Section Imaging Using the Transmission Electron Microscopy.** For cell cross-section imaging, GSH-AuNP incubated cells were first detached from the well plate. After a wash with PBS, at least $5 \times 10^5$ cells were fixed for 2 h with modified Karnovsky's fixative (2% paraformaldehyde and 2% glutaraldehyde in 0.05 M sodium cacodylate buffer, pH 7.2). After three washings with 0.05 M sodium cacodylate buffer (pH 7.2) at 4 °C, cells were fixed with 1% osmium tetroxide in 0.05 M sodium cacodylate buffer (pH 7.2) for 2 h and then washed with distilled water two times. Fixed cells were En bloc stained at 4 °C for overnight using 0.5% uranyl acetate and then dehydrated with a graded concentration series of ethanol (30%, 50%, 70%, 80%, 90%, 100%, 100%, and 100% ethanol; 10 min for each dehydration step). Infiltrated cells using propylene oxide and Spurr's resin were polymerized at 70 °C for 24 h. Various sections of the resin block were cut using the ultramicrotome (MT-X, RMC, Tucson, AZ, USA) and stained 2% uranyl acetate and Reynolds' lead citrate for 7 min, followed by transferring the section of interest onto a 300 mesh copper TEM grid.

**Toxicity Assay.** The cytotoxicity of various concentrations of GSH-AuNPs was evaluated using the Cell Counting Kit (CCK-8, Dojindo lab., Japan). Cells were grown in a 96-well plate in 100 $\mu$L of DMEM supplemented with FBS. After 24 h seeding, cells were incubated with various concentrations (from 2 nM to 200 $\mu$M) of glutathione-modified gold probes for 48 h, and cell viability assay was carried out. The metabolic activity of the cells was measured using CCK-8 (a sensitive colorimetric assay for the determination of the number of viable cells after incubating with probes).[55] Then, 10 $\mu$L of the CCK-8 solution was directly added to the incubated cells in each well. After 2 h incubation at 37 °C, the amount of formazan dyes, generated by dehydrogenased of active cells, was measured by a microplate reader (Anthos 2010, Anthos Labtec, Eugendorf, Austria).

**Cell Lysis.** For cell lysis, well grown cells were detached from a well plate using TrypLETM Express (1X, Gibco, Invitrogen, USA). After being perfectly washed with DPBS, the same number of cells ($5 \times 10^5$ cells in this case) was incubated with 200 $\mu$L of cell lysis buffer (M-PER mammalian protein extraction reagent, Pierce, Rockford, IL, USA) with gentle shaking for 10 min. After cell debris was removed by simple centrifugation (~14 000*g* for 5 min), the supernatant was transferred to a new eppendorf tube for the assay that followed.

**Detection of ROS from Cells.** To compare the ROS level of different type of cells, three types of cancer cells [HeLa (human cervical cancer cell), A549 (human lung cancer cell) and Hep3B (human hepatoma cell)] and three types of normal cells [3T3-L1 (fibroblast cell), NIH3T3 (fibroblast cell), and C2C12 (myoblast cell)] were cultured in Dulbecco's Modified Eagle's Medium (DMEM) (GIBCO, Invitrogen Inc., Carlsbad, CA, USA), supplemented with 10% (v/v) Fetal Bovine Serum (FBS) (GIBCO, Invitrogen Inc., Carlsbad, CA, USA) and 5% penicillin/streptomycin (Sigma-Aldrich). After 3 days of culturing, cells were detached from the culturing flasks with trypsin EDTA (Gibco, Invitrogen Inc., Carlsbad, CA, USA). The cells were then washed with PB (10 mM, pH 7.4) three times. The cells (~$5 \times 10^5$ cells) were incubated with 47 nM GSH-AuNPs in 90 $\mu$L of PB (10 mM, pH 7.4) followed by the addition of 10 mM ferrous chloride (10 $\mu$L) to the solution to generate more detectable ROS radical species. After 4 h incubation and subsequent centrifugation at 2000 rpm for 3 min, 60 $\mu$L of the supernatant was collected for UV−vis analysis. UV−vis absorbance spectra of GSH-AuNP-cell mixtures were recorded for each cell line, and the respective supernatant from a cell-cultured solution was used as a blank.

**Commercial *in Vitro* ROS/RNS Assay.** To validate our GSH-AuNP-based cell assay results, the results from commercially available OxiSelect *In Vitro* ROS/RNS Assay Kit were compared. The OxiSelect assay is a fluorescence-based method in which fluorescence intensity is proportional to the total ROS/RNS level within

the sample. This assay utilizes a proprietarily quenched fluorogenic probe, dichlorodihydrofluorescin DiOxyQ (DCFH-DiOxyZ), which can specifically detect ROS/RNS. The DCFH-DiOxyZ can be transformed to the highly reactive fluorescence-quenched DCFH form, and the quenched fluorescence signal from the DCFH can be turned on upon ROS/RNS detection. The same number of cells ($5 \times 10^5$ cells) was used for all the experiments after cell detachment from the culture dish and cell lysis. Next, 50 $\mu$L of cell lysate was added to a 96-well plate (30096, SPL lifescience, Gyeonggi-Do, South Korea), suitable for fluorescence measurement. DCFH can be highly reactive to ROS/RNS by mixing 50 $\mu$L of catalyst with 100 $\mu$L of the DCFH solution (DCFH-DiOxyQ, priming reagent and stabilization solution with the recommended ratio by the manufacturer). After 45 min incubation at room temperature with gentle shaking, the fluorescence signal, which is proportional to the ROS/RNS level, can be obtained using a fluorescence plate reader (The SynergyHT, BioTek, VT, USA) with 480 nm excitation and 530 nm emission.

*Conflict of Interest:* The authors declare no competing financial interest.

*Acknowledgment.* J.-M.N. was supported by the National Research Foundation of Korea (NRF) grant funded by the Korean government (MEST) (No. 2011-0018198) and the Pioneer Research Center Program through the National Research Foundation of Korea funded by the Ministry of Education, Science and Technology (2012-0009565). The authors would also like to acknowledge financial support from the Industrial Core Technology Development Program of the Ministry of Knowledge Economy (No. 10033183 and No. 10037397).

*Supporting Information Available:* Experimental procedures, some spectra, and TEM images of different ligand-capped Au nanoparticles. This material is available free of charge *via* the Internet at http://pubs.acs.org.

## REFERENCES AND NOTES

1. Autréaux, B. D.; Toledano, M. B. ROS as Signalling Molecules: Mechanisms that Generate Specificity in ROS Homeostasis. *Nat. Rev. Mol. Cell Biol.* **2007**, *8*, 813–824.
2. Valko, M.; Leibfritz, D.; Moncol, J.; Cronin, M. T.; Mazur, M.; Telser, J. Free Radicals and Antioxidants in Normal Physiological Functions and Human Disease. *Int. J. Biochem. Cell Biol.* **2007**, *39*, 44–84.
3. Winterbourn, C. C. Reconciling the Chemistry and Biology of Reactive Oxygen Species. *Nat. Chem. Biol.* **2008**, *4*, 278–286.
4. Nel, A.; Xia, T.; Madler, L.; Li, N. Toxic Potential of Materials at the Nanolevel. *Science* **2006**, *311*, 622–627.
5. Chen, X.; Tian, X.; Shin, I.; Yoon, J. Fluorescent and Luminescent Probes for Detection of Reactive Oxygen and Nitrogen Species. *Chem. Soc. Rev.* **2011**, *40*, 4783–4804.
6. Tang, Y.; Feng, F.; He, F.; Wang, S.; Li, Y.; Zhu, D. Direct Visualization of Enzymatic Cleavage and Oxidative Damage by Hydroxyl Radicals of Single-Stranded DNA with a Cationic Polythiophene Derivative. *J. Am. Chem. Soc.* **2006**, *128*, 14972–14976.
7. Shen, Q.; Nie, Z.; Guo, M.; Zhong, C.-J.; Lin, B.; Li, W.; Yao, S. Simple and Rapid Colorimetric Sensing of Enzymatic Cleavage and Oxidative Damage of Single-Stranded DNA with Unmodified Gold Nanoparticles as Indicator. *Chem. Commun.* **2009**, *8*, 929–931.
8. Jiang, H.; Ju, H. Electrochemiluminescence Sensors for Scavengers of Hydroxyl Radical Based on Its Annihilation in CdSe Quantum Dots Film/Peroxide System. *Anal. Chem.* **2007**, *79*, 6690–6696.
9. Gill, R.; Bahshi, L.; Freeman, R.; Willner, I. Optical Detection of Glucose and Acetylcholine Esterase Inhibitors by $H_2O_2$-Sensitive CdSe/ZnS Quantum Dots. *Angew. Chem., Int. Ed.* **2008**, *120*, 1676–1679.
10. Hu, M.; Tian, J.; Lu, H.-T.; Weng, L.-X; Wang, L.-H. $H_2O_2$-Sensitive Quantum Dots for the Label-Free Detection of Glucose. *Talanta* **2010**, *82*, 997–1002.
11. Uusitalo, L. M.; Hempel, N. Recent Advances in Intracellular and *in Vivo* ROS Sensing: Focus on Nanoparticle and Nanotube Applications. *Int. J. Mol. Sci.* **2012**, *13*, 10660–10679.
12. Rosi, N. L.; Mirkin, C. A. Nanostructures in Biodiagnostics. *Chem. Rev.* **2005**, *105*, 1547–1562.
13. Lee, J.-S.; Han, M. S.; Mirkin, C. A. Colorimetric Detection of Mercuric Ion ($Hg^{2+}$) in Aqueous Media using DNA-Functionalized Gold Nanoparticles. *Angew. Chem., Int. Ed.* **2007**, *46*, 4093–4096.
14. Wilson, R. The Use of Gold Nanoparticles in Diagnostics and Detection. *Chem. Soc. Rev.* **2008**, *37*, 2028–2045.
15. Georganopoulou, D. G.; Chang, L.; Nam, J.-M.; Thaxton, C. S.; Mufson, E. J.; Klein, W. L.; Mirkin, C. A. Nanoparticle-Based Detection in Cerebral Spinal Fluid of a Soluble Pathogenic Biomarker for Alzheimer's Disease. *Proc. Natl. Acad. Sci. U.S.A.* **2005**, *102*, 2273–2276.
16. Neely, A.; Perry, C.; Varisli, B.; Singh, A. K.; Arbneshi, T.; Senapati, D.; Kalluri, J. R.; Ray, P. C. Ultrasensitive and Highly Selective Detection of Alzheimer's Disease Biomarker Using Two-Photon Rayleigh Scattering Properties of Gold Nanoparticle. *ACS Nano* **2009**, *3*, 2834–2840.
17. Kong, B.; Zhu, A.; Luo, Y.; Tian, Y.; Yu, Y.; Shi, G. Sensitive and Selective Colorimetric Visualization of Cerebral Dopamine Based on Double Molecular Recognition. *Angew. Chem., Int. Ed.* **2011**, *50*, 1837–1840.
18. Jiang, Y.; Zhao, H.; Zhu, N.; Lin, Y.; Yu, P.; Mao, L. A Simple Assay for Direct Colorimetric Visualization of Trinitrotoluene at Picomolar Levels Using Gold Nanoparticles. *Angew.Chem. Int. Ed.* **2008**, *47*, 8601–8604.
19. Kalluri, J. R.; Arbneshi, T.; Khan, S. A.; Neely, A.; Candice, P.; Varisli, B.; Washington, M.; McAfee, S.; Robinson, B.; Banerjee, S.; *et al*. Use of Gold Nanoparticles in a Simple Colorimetric and Ultrasensitive Dynamic Light Scattering Assay: Selective Detection of Arsenic in Groundwater. *Angew. Chem., Int. Ed.* **2009**, *48*, 9668–9671.
20. Chi, H.; Liu, B.; Guan, G.; Zhang, Z.; Han, M.-Y. A Simple, Reliable and Sensitive Colorimetric Visualization of Melamine in Milk by Unmodified Gold Nanoparticles. *Analyst* **2010**, *135*, 1070–1075.
21. Laromaine, A.; Koh, L.; Murugesan, M.; Ulijn, R. V.; Stevens, M. M. Protease-Triggered Dispersion of Nanoparticle Assemblies. *J. Am. Chem. Soc.* **2007**, *129*, 4156–4157.
22. Kong, B.; Zhu, A.; Luo, Y.; Tian, Y.; Yu, Y.; Shi, G. Sensitive and Selective Colorimetric Visualization of Cerebral Dopamine Based on Double Molecular Recognition. *Angew. Chem., Int. Ed.* **2011**, *50*, 1837–1840.
23. Lim, D.-K.; Jeon, K.-S.; Kim, H.-M.; Nam, J.-M.; Suh, Y. D. Highly Uniform and Reproducible Surface-Enhanced Raman Scattering from DNA-Tailorable Nanoparticles with 1-nm Interior Gap. *Nat. Nanotechnol.* **2011**, *6*, 452–460.
24. Woo, J.-R.; Lim, D.-K.; Nam, J.-M. Minimally Stable Nanoparticle-Based Colorimetric Assay for Simple, Rapid, and Sensitive Antibody Structure and Activity Evaluation. *Small* **2011**, *7*, 648–655.
25. Jang, K.-J.; Lee, H.; Jin, H.-L.; Park, Y.; Nam, J.-M. Restriction-Enzyme-Coded Gold-Nanoparticle Probes for Multiplexed DNA Detection. *Small* **2009**, *5*, 2665–2668.
26. Lim, D.-K.; Jeon, K.-S.; Kim, H. M.; Nam, J.-M.; Suh, Y. D. Nanogap-Engineerable Raman-Active Nanodumbbells for Single-Molecule Detection. *Nat. Mater.* **2010**, *9*, 60–67.
27. Shiang, Y.-C.; Huang, C.-C.; Chang, H.-T. Gold Nanodot-Based Luminescent Sensor for the Detection of Hydrogen Peroxide and Glucose. *Chem. Commun.* **2009**, *23*, 3437–3439.
28. Jv, Y.; Li, B.; Cao, R. Positively-Charged Gold Nanoparticles as Peroxidiase Mimic and Their Application in Hydrogen Peroxide and Glucose Detection. *Chem. Commun.* **2010**, *46*, 8017–8019.
29. Jiang, Y.; Zhao, H.; Lin, Y.; Zhu, N.; Ma, Y.; Mao, L. Colorimetric Detection of Glucose in Rat Brain Using Gold Nanoparticles. *Angew. Chem., Int. Ed.* **2010**, *49*, 4800–4804.
30. Lee, H.; Lee, K.; Kim, I. K.; Park, T. G. Fluorescent Gold Nanoprobe Sensitive to Intracellular Reactive Oxygen Species. *Adv. Funct. Mater.* **2009**, *19*, 1884–1890.
31. Auchinvole, C. A. R.; Richardson, P.; McGuinnes, C.; Mallikarjun, V.; Donaldson, K.; McNab, H.; Campbell, C. J.

Monitoring Intracellular Redox Potential Changes Using SERS Nanosensors. *ACS Nano* **2012**, *6*, 888–896.
32. Polavarapu, L.; Manna, M.; Xu, Q.-H. Biocompatible Glutathione Capped Gold Clusters as One- and Two-Photon Excitation Fluorescence Contrast Agents for Live Cells Imaging. *Nanoscale* **2011**, *3*, 429–434.
33. Brinas, R. P.; Hu, M.; Qian, L.; Lymar, E. S.; Hainfeld, J. F. Gold Nanoparticle Size Controlled by Polymeric Au(I) Thiolate Precursor Size. *J. Am. Chem. Soc.* **2008**, *130*, 975–982.
34. Wu, Q.; Cao, H.; Luan, Q.; Zhang, J.; Wang, Z.; Warner, J.-H.; Watt, A. R. Biomolecule-Assisted Synthesis of Water-Soluble Silver Nanoparticles and Their Biomedical Applications. *Inorg. Chem.* **2008**, *47*, 5882–5888.
35. Blair, I. A. Analysis of Endogenous Glutathione-Adducts and Their Metabolites. *Biomed. Chromatogr.* **2010**, *24*, 29–38.
36. Awasthi, Y. C.; Sharma, R.; Yadav, S.; Dwivedi, S.; Sharma, A.; Awasthi, S. The Non-ABC Drug Transporter RLIP76 (RALBP-1) Plays a Major Role in the Mechanisms of Drug Resistance. *Curr. Drug Metab.* **2007**, *8*, 315–323.
37. He, X.; Zhong, Z.; Guo, Y.; Lv, J.; Xu, J.; Zhu, M.; Li, Y.; Liu, H.; Wang, S.; Zhu, Y.; *et al.* Gold Nanoparticle-Based Monitoring of the Reduction of Oxidized to Reduced Glutathione. *Langmuir* **2007**, *23*, 8815–8819.
38. Imlay, J. A. Pathways of Oxidative Damage. *Annu. Rev. Microbiol.* **2003**, *57*, 395–418.
39. Page, S. E.; Wilke, K. T.; Pierre, V. C. Sensitive and Selective Time-Gated Luminescence Detection of Hydroxyl Radical in Water. *Chem. Commun.* **2010**, *46*, 2423–2425.
40. Bhandari, A.; Kim, W.; Hohn, K. Luminol-Based Enhanced Chemiluminescence Assay for Quantification of Peroxidase and Hydrogen Peroxide in Aqueous Solutions: Effect of Reagent pH and Ionic Strength. *J. Environ. Eng.* **2010**, *136*, 1147–1152.
41. Niidome, T.; Nakashima, K.; Takahashi, H.; Niidome, Y. Preparation of Primary Amine-Modified Gold Nanoparticles and Their Transfection Ability into Cultivated Cells. *Chem. Commun.* **2004**, *17*, 1978–1979.
42. Abad, J. M.; Mertens, S. F. L.; Pita, M.; Fernandez, V. M.; Schiffrin, D. J. Functionalization of Thioctic Acid-Capped Gold Nanoparticles for Specific Immobilization of Histidine-Tagged Proteins. *J. Am. Chem. Soc.* **2007**, *129*, 4156–4157.
43. Sarangi, S. N.; Hussain, A. M. P.; Sahu, S. N.; Strong, U. V. Absorption and Emission from L-cysteine Capped Monodispersed Gold Nanoparticles. *Appl. Phys. Lett.* **2009**, *95*, 0731091–0731093.
44. Jones, D. P. Redox potential of GSH/GSSG couple: Assay and Biological Significance. *Methods Enzymol* **2002**, *348*, 93–112.
45. Kirlin, W. G.; Cai, J.; Thompson, S. A.; Diaz, D.; Kavanagh, T. J.; Jones, D. P. Glutathione Redox Potential in Response to Differentiation and Enzyme Inducers. *Free Radical Biol. Med.* **1999**, *27*, 1208–1218.
46. Kumar, B.; Koul, S.; Khandrika, L. Oxidative Stress Is Inherent in Prostate Cancer Cells and Is Required for Aggressive Phenotype. *Cancer Res.* **2008**, *68*, 1777–1785.
47. Trachootham, D.; Alexandre, J.; Huang, P. Targeting Cancer Cells by ROS-Mediated Mechanisms: A Radical Therapeutic Approach? *Nat. Rev. Drug Discovery* **2009**, *8*, 579–591.
48. Kim, J.-W.; Dang, C. V. Cancer's Molecular Sweet Tooth and the Warburg Effect. *Cancer Res.* **2006**, *66*, 8927–8930.
49. EO, H.; Liu, J.; Alvitar, M.; Keating, M. J.; Huang, P. Intrinsic Oxidative Stress in Cancer Cells: A Biochemical Basis for Therapeutic Selectivity. *Cancer Chemother. Pharmacol.* **2004**, *53*, 209–219.
50. Szatrowski, T. P.; Nathan, C. F. Production of Large Amounts of Hydrogen Peroxide by Human Tumor Cells. *Cancer Res.* **1991**, *51*, 794–798.
51. Weinberg, F.; Chandel, N. S. Reactive Oxygen Species-Dependent Signaling Regulates Cancer. *Cell. Mol. Life. Sci.* **2009**, *66*, 3663–3673.
52. Pelicano, H.; Carneya, D.; Huang, P. ROS Stress in Cancer Cells and Therapeutic Implications. *Drug Resist. Update* **2004**, *7*, 97–110.
53. Raj, L.; Ide, T.; Gurkar, A. U.; Foley, M.; Schenone, M.; Li, X.; Tolliday, N. J.; Golub, T. R.; Carr, S. A.; Shamji, A. F.; *et al.* Selective Killing of Cancer Cells by a Small Molecule Targeting the Stress Response to ROS. *Nature* **2011**, *475*, 231–234.
54. Rosi, N. L.; Giljohann, D. A.; Thaxton, C. S.; Lytton-Jean, A. K. R.; Han, M. S.; Mirkin, C. A. Oligonucleotide-Modified Gold Nanoparticles for Intracellular Gene Regulation. *Science* **2006**, *19*, 1027–1030.
55. Ishiyama, M.; Miyazono, Y.; Sasamoto, K.; Ohkura, Y.; Ueno, K. A Highly Water-Soluble Disulfonated Tetrazolium Salt as a Chromogenic Indicator for NADH as Well as Cell Viability. *Talanta* **1997**, *44*, 1299–305.
56. Keston, A. S.; Brandt, R. The Fluorometric Analysis of Ultramicro-quantities of Hydrogen Peroxide. *Anal. Biochem.* **1965**, *11*, 1–5.